

Anomalous Zero-Field Splitting for Hole Spin Qubits in Si and Ge Quantum Dots

Bence Hetényi¹,* Stefano Bosco¹, and Daniel Loss

Department of Physics, University of Basel, Klingelbergstrasse 82, CH-4056 Basel, Switzerland



(Received 5 May 2022; accepted 15 August 2022; published 9 September 2022)

An anomalous energy splitting of spin triplet states at zero magnetic field has recently been measured in germanium quantum dots. This zero-field splitting could crucially alter the coupling between tunnel-coupled quantum dots, the basic building blocks of state-of-the-art spin-based quantum processors, with profound implications for semiconducting quantum computers. We develop an analytical model linking the zero-field splitting to the Rashba spin-orbit interaction that is cubic in momentum. Such interactions naturally emerge in hole nanostructures, where they can also be tuned by external electric fields, and we find them to be particularly large in silicon and germanium, resulting in a significant zero-field splitting in the μeV range. We confirm our analytical theory by numerical simulations of different quantum dots, also including other possible sources of zero-field splitting. Our findings are applicable to a broad range of current architectures encoding spin qubits and provide a deeper understanding of these materials, paving the way toward the next generation of semiconducting quantum processors.

DOI: [10.1103/PhysRevLett.129.116805](https://doi.org/10.1103/PhysRevLett.129.116805)

Introduction.—The compatibility of localized spins in semiconducting quantum dots (QDs) [1] with the well-developed CMOS technology is pushing these architectures to the front of the race toward the implementation of scalable quantum computers [2–7]. Spin qubits based on hole states in silicon (Si) and germanium (Ge), in particular, are gaining increasing attention in the community [6,7] because of their large spin-orbit interaction (SOI) [8–11], enabling fast and power-efficient all-electric gates [12–15] and strong transversal and longitudinal coupling to microwave resonators [16–20]. Also, significant steps forward in material engineering [21,22] as well as fast spin readout and qubit initialization protocols [23–26] facilitated the implementation of high-fidelity 2-qubit gates [27,28] and of a 4-qubit quantum processor with controllable qubit-qubit couplings [29].

In contrast to electrons, the properties of hole QDs depend on the mixing of two bands, the heavy-hole (HH) and light-hole (LH) bands, resulting in several unique features that are beneficial for quantum computing applications [30–37]. In addition to the large and externally controllable SOI [8,30,35], that can be conveniently engineered to be linear or cubic in momentum [9,31,38–41], hole spin qubits also feature highly anisotropic and electrically tunable g factors [42–47], hyperfine interactions [37], and anisotropies of exchange interaction at finite magnetic fields [33]. Because HHs and LHs are strongly mixed in quasi-one-dimensional (1D) systems, these effects are significantly enhanced in long QDs.

Recent experiments in Ge QDs with even hole occupation have also detected a large anomalous lifting of the threefold degeneracy of triplet states at zero magnetic field [48], yielding another striking difference between electrons

and holes. A similar zero-field splitting (ZFS) has been reported in other quantum systems e.g., divacancies in silicon carbide [49], nitrogen vacancies in diamond [50,51], and carbon nanotubes [52]. Nevertheless, after two decades of intense research, the experiment of Ref. [48] is the first record of the ZFS in any QD system, but the physical mechanism behind this effect remains unexplained. In this Letter, we discuss the microscopic origin of the exchange anisotropy in hole QDs and we propose a general theory modeling the ZFS in a wide range of devices. Our theory helps to develop a fundamental understanding of ZFS, essential to account for its effect in quantum computing applications. For example, the exchange anisotropy associated with the ZFS could enable the encoding of hole singlet-triplet qubits [53–56] at zero magnetic field, and when combined with a Zeeman field it can lift the Pauli spin blockade [57,58], with critical implications in readout protocols. Furthermore, ZFS can introduce systematic errors in 2-qubit gates based on isotropic interactions between tunnel-coupled QDs [1,33,59].

We associate the large ZFS emerging in hole QDs to the cubic-in-momentum Rashba SOI [31,32]. As opposed to the zinc blende crystals (e.g., GaAs, InAs), where the broken bulk inversion symmetry gives rise to Dresselhaus SOI terms that are to lowest order cubic in momentum, the cubic Rashba term is an often neglected correction to the well-known linear contribution. Rashba SOI is a natural candidate to explain exchange anisotropies; however, its dominant contribution—linear in momentum—can be gauged away in quasi-1D systems [60–62] and cannot lift the triplet degeneracy without magnetic fields. While in electronic systems only the linear SOI is sizable, in hole nanostructures the large mixing of HHs and LHs induces a

large cubic SOI [31,32] yielding a significant ZFS in Si and Ge QDs. Strikingly, this ZFS is tunable by external electric fields and can be engineered by the QD design.

We develop a theory for the cubic-SOI-induced ZFS that relies exclusively on single-particle properties of the QD and the Bohr radius, providing an accurate estimate of the ZFS in a wide range of common architectures. In realistic systems, this ZFS is in the μeV range, orders of magnitude larger than alternative mechanisms. For example, we find that ZFS of a few neV can also be induced by short-range corrections of the Coulomb interaction arising from the p -type orbital wave functions of the valence band [36,63]. In addition, our theory relates the axis of the exchange anisotropy to the direction of the SOI, and corroborates the observed response of the QDs to small magnetic fields [48]. Importantly, because in a long QD comprising two holes the Coulomb repulsion of the two particles leads to a formation of Wigner molecule [64–67] that is analogous to a double QD in one-dimensional systems, our theory describes the exchange anisotropy also in tunnel-coupled QDs, the prototypical building blocks of current spin-based quantum processors [33,59,68], and thus our findings have profound implications in the growing research field of quantum computing with holes.

Analytical theory.—Large SOI emerges naturally in hole spin qubits encoded in long quantum dots, where the confinement potential in two directions is stronger than in the third one. Such nanostructures include a wide range of common spin qubit architectures, such as Si fin field effect transistors (finFETs) [25,30,35,69], squeezed QDs in planar Ge [39], and Si and Ge nanowires (NWs) [8,10,66,70]. Their response is well described by an effective 1D low-energy Hamiltonian acting only on a few subbands.

We now focus on a QD defined in a NW with a square cross section of side L . By resorting to Schrieffer-Wolff perturbation theory [71] discussed in detail in Sec. S1 of Ref. [72], we find the effective Hamiltonian acting on the lowest pair of subbands as

$$H_1 = \frac{p_z^2}{2m^*} + v p_z \sigma^y + v_3 p_z^3 \sigma^y + \frac{\hbar^2}{2m^* l_z^4} z^2, \quad (1)$$

up to third order in the momentum p_z in the long direction. Here, m^* is the effective mass, v and v_3 are the linear and cubic SOI, respectively, and σ^y is a Pauli matrix. The cubic SOI term is typically strongly suppressed compared to the subband splitting $\Delta_{\text{sub}} \sim \hbar^2/2m^*L^2$, i.e., $v_3(\hbar/L)/\Delta_{\text{sub}} \sim 10^{-3} - 0.05$, whereas the linear term can be extremely strong for hole states, i.e., $v(\hbar/L)/\Delta_{\text{sub}} \sim 1-10$ [8–11]. The QD is defined by a harmonic potential parametrized by the length l_z and modeling the smooth electrostatic confinement produced by metallic gates. Equation (1) is valid when $l_z \gtrsim L/\pi$. Two holes confined in the same QD are described by the Hamiltonian $H_2 = H_1^{(1)} + H_1^{(2)} + V_c^{(1,2)}$,

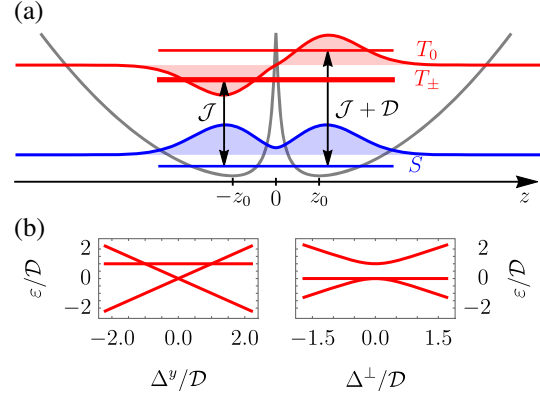


FIG. 1. Exchange interaction in long quantum dots. (a) The effective 1D potential $\Delta_0(z_1 - z_2)^2/4l_z^2 + V_c(z_1 - z_2)$ is shown in gray (without units) as a function of relative coordinate $z = z_1 - z_2$, where $\pm z_0$ are the minima of the potential. The energy levels corresponding to the lowest singlet and triplet states and the corresponding orbital wave functions are overlaid with blue and red, respectively. Vertical arrows show the definition of the exchange splitting and ZFS, \mathcal{J} and \mathcal{D} , respectively. Note that the energy scale of the singlet-triplet energy levels is only schematic, not matched with that of the effective potential. (b) Splitting ε of the three triplet states when the Zeeman field is aligned with the SOI (Δ^y , left-hand panel), and when it is perpendicular to it (Δ^\perp , right-hand panel).

where $V_c^{(1,2)}$ is the effective Coulomb potential in the lowest subband sector. Coulomb interactions with higher subbands are negligible when $L/\pi < a_B$, where $a_B = 4\pi\epsilon_r\hbar^2/m^*e^2$ is the effective Bohr radius with ϵ_r being the dielectric constant of the material. The Coulomb potential $V_c^{(1,2)}$ together with the effective harmonic potential acting on the relative coordinate $(\hbar^2/4m^*l_z^4)(z_1 - z_2)^2$ is sketched in Fig. 1(a) and is discussed in Ref. [72].

The linear SOI v in Eq. (1) can be eliminated exactly by a spin-dependent shift of momentum that leaves the potential unchanged, and only negligibly renormalizes the effective mass m^* [72]. The two-particle Hamiltonian is then given by

$$H_2 = \frac{1}{4m^*} P^2 + \frac{\hbar^2}{m^* l_z^4} Z^2 + \frac{1}{m^*} p^2 + \frac{\hbar^2}{4m^* l_z^4} z^2 + V_c(z) + \mathcal{P}_3^+(\sigma_1^y + \sigma_2^y) + \mathcal{P}_3^-(\sigma_1^y - \sigma_2^y), \quad (2)$$

where $Z = (z_1 + z_2)/2$ is the center-of-mass (c.m.) coordinate with conjugate momentum $P = p_{z_1} + p_{z_2}$, and $z = z_1 - z_2$ is the relative coordinate with momentum $p = (p_{z_1} - p_{z_2})/2$. The cubic SOI yields the perturbative corrections $\mathcal{P}_3^+ = v_3(\frac{1}{8}P^3 + \frac{3}{2}Pp^2)$ and $\mathcal{P}_3^- = v_3(\frac{3}{4}P^2p + p^3)$ in the second line of Eq. (2); these terms mix relative and c.m. coordinates and are crucial for the ZFS.

At $v_3 = 0$, the Hamiltonian of the c.m. coordinates is a harmonic oscillator with an orbital energy $\Delta_o = \hbar^2/m^*l_z^2$,

while the Hamiltonian of the relative coordinates is $H_{\text{rel}} = p^2/m^* + \hbar^2 z^2/4m^*l_z^4 + V_c(z)$. In a NW with a square cross section and when $l_z \gtrsim a_B$, the effective 1D Coulomb interaction is well approximated by $V_c(z) \approx \Delta_o [z^2 + (L/4)^2]^{-1/2} l_z^2/a_B$, where $L/4$ is a short-range cutoff of the potential derived in Sec. S1.1 of Ref. [72]. In this case, the system is fully described by two relative length scales l_z/a_B and L/a_B . Because the effective potential in H_{rel} is an even function of z , the corresponding eigenfunctions have either even or odd parity, enabling the distinction between singlets (even) and triplets (odd) states.

While in this work we focus on a single QD occupied by two holes, we emphasize that our theory is also valid for two tunnel-coupled QDs, the basic components of current spin-based quantum processors [28,29]. In fact, as sketched in Fig. 1(a), in a doubly occupied long QD, with $l_z \gtrsim a_B$, the Coulomb repulsion forces the two particles toward opposite ends of the dot [64–66], effectively resulting in two coupled dots. That is why the distinct peak of the effective two-particle potential, i.e., $V_c(0) \approx 4\Delta_o l_z^2/a_B L$, is comparable to the orbital splitting. We also remark that because $a_B \sim 12$ nm ($a_B \sim 3$ nm) in Ge (Si), the condition $l_z \gtrsim a_B$ of long QDs is typically respected in current experimental setups [15,48,73].

By a second-order Schrieffer-Wolff transformation [71] and projecting the two-particle Hamiltonian onto the lowest-energy singlet and triplet states, we find that the exchange Hamiltonian is

$$H_{\text{eff}} = \frac{1}{4}(\mathcal{J} + \mathcal{D})\boldsymbol{\sigma}_1 \cdot \boldsymbol{\sigma}_2 - \frac{1}{2}\mathcal{D}\sigma_1^y\sigma_2^y + \frac{1}{2}\boldsymbol{\Delta}^\perp \cdot (\boldsymbol{\sigma}_1^\perp + \boldsymbol{\sigma}_2^\perp) + \frac{1}{2}\Delta^y(\sigma_1^y + \sigma_2^y), \quad (3)$$

where Δ^y is the Zeeman field parallel to the SOI, while $\boldsymbol{\Delta}^\perp = (\Delta^x, \Delta^z)$ are components perpendicular to it. The exchange splitting $\mathcal{J} = \varepsilon_{T_\pm} - \varepsilon_S > 0$ only weakly depends on v_3 and it is well approximated by $\mathcal{J}_0 = \zeta \hbar^2 a_B^2/m^* l_z^4$, the energy gap between the lowest odd and even eigenstates of the relative coordinate Hamiltonian. We introduce the dimensionless coefficient $\zeta \sim 0.3$ – 1 for $0.8 < L/a_B < 2$ and $a_B \lesssim l_z$ [72]. Note that the ZFS appears in Hamiltonian (3) as a spin-spin interaction term ($\propto \sigma_1^y\sigma_2^y$). Therefore, as discussed in the following, it originates from the interplay of many-particle Coulomb interaction and the cubic Rashba SOI.

Without magnetic fields, $\Delta^i = 0$ and Eq. (3) correspond to an exchange Hamiltonian with a uniaxial anisotropy; i.e., $J_{xx} = J_{zz} = \mathcal{J}$ and the anisotropy axis is aligned to the SOI (i.e., y direction) with $J_{yy} = \mathcal{J} + \mathcal{D}$. As sketched in Fig. 1(a), the ZFS \mathcal{D} lifts the degeneracy of the triplets T_\pm and T_0 , where the three triplets $T_{\pm,0}$ are defined with quantization axis along the y direction. From perturbation theory, we obtain [72]

$$\mathcal{D} = m^* v_3^2 \frac{\hbar^4}{l_z^4} \eta. \quad (4)$$

Here the dimensionless coefficient $\eta \sim 0.4$ – 0.8 includes various combinations of dimensionless momentum matrix elements. The exact functional dependence of η and ζ on L and l_z is discussed in detail in Sec. S1.1 of Ref. [72]. Because η depends only weakly on the relative length scales l_z/a_B and L/a_B in long QDs, to good approximation we find that $\mathcal{D} \propto l_z^{-4}$. We also emphasize that this ZFS is strongly dependent on the cubic SOI and it requires a sizable value of v_3 , achievable only in hole QDs. The relative anisotropy of the exchange interactions is

$$\frac{\mathcal{D}}{\mathcal{J}} = \frac{m^* v_3^2 \hbar^2 \eta}{a_B^2 \zeta}, \quad (5)$$

where $\eta/\zeta \sim 1$ – 5 depends weakly on a_B and, therefore, the anisotropy scales as $\mathcal{D}/\mathcal{J} \propto (m^*)^4$.

The magnetic field dependence of the triplet states can also be deduced straightforwardly from Eq. (3) and it is sketched in Fig 1(b). If the magnetic field is applied parallel to the SOI (i.e., the anisotropy axis) the nondegenerate triplet T_0 is unaffected by the field and $\varepsilon_{T_0} = \mathcal{J} + \mathcal{D}$, whereas the degenerate triplets T_\pm split linearly with the Zeeman field as $\varepsilon_{T_\pm} = \mathcal{J} \pm \Delta^y$. In contrast, if the field is applied perpendicular to the SOI, one of the degenerate triplets, e.g., T'_0 , stays at the same energy $\varepsilon_{T'_0} = \mathcal{J}$, while the remaining triplets T'_\pm split quadratically as $\varepsilon_{T'_\pm} = \mathcal{J} + \mathcal{D}/2 \pm \sqrt{\mathcal{D}^2/4 + |\Delta^\perp|^2}$ at small Zeeman fields. This signature of the exchange anisotropy is consistent with recent experimental observations in Ref. [48], supporting our theory of ZFS in Ge hut wires.

Numerics.—We confirm our analytical results by comparing them with a numerical simulation of long QDs in square Ge and Si NWs with side length L based on the six-band Kane model [74]. By imposing hard-wall boundary conditions at the edge of the NW cross section, we obtain an effective 1D model including several transversal subbands. With a third-order Schrieffer-Wolff transformation, we then fold the higher-energy subbands down to the lowest four subbands, also accounting for terms that are cubic in momentum. We emphasize that in contrast to our analytical treatment, where we only account for a single pair of subbands, see Eq. (1), our numerical treatment also includes a pair of higher-energy subbands [72]. Furthermore, we include Coulomb interaction matrix elements that couple different subbands, as well as short-range interband corrections to the Coulomb interaction [36], that we identify as an alternative source of ZFS. In our simulation, we also consider a compressive strain along the wire, with $\varepsilon_{zz} = -0.5\%$, ensuring that the lowest band has a positive effective mass [8,30]. More details on the numerical simulation are provided in Sec. S2 of Ref. [72],

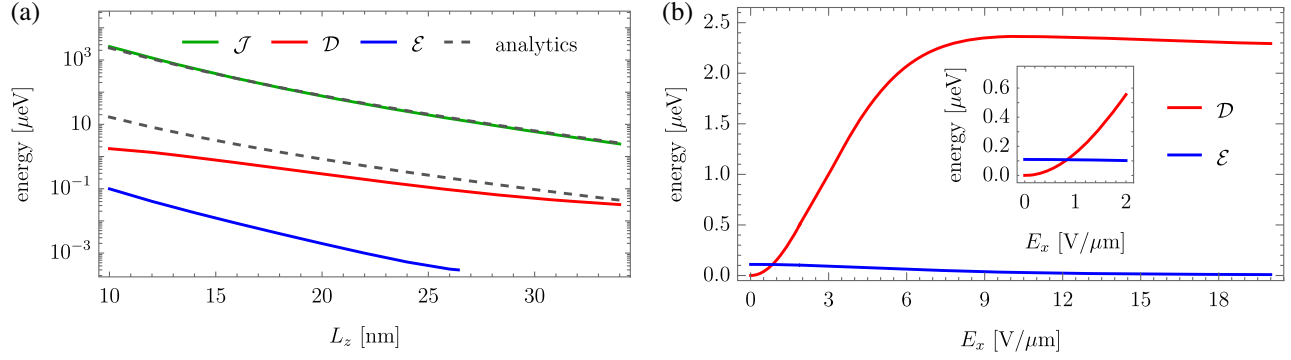


FIG. 2. Anisotropic exchange interactions in Ge. (a) Exchange splitting \mathcal{J} and ZFSs \mathcal{D} and \mathcal{E} in a Ge square NW with side length $L = 10$ nm and compressive strain $\epsilon_{zz} = -0.5\%$, as a function of QD length L_z for $E_x = 5$ $\text{V}/\mu\text{m}$; the analytical results of the corresponding quantities are shown in dashed lines. Here the QD length is defined as $L_z = (m^*\gamma_1/m_e)^{1/4}l_z \approx l_z$, where m_e/γ_1 is the averaged hole mass with m_e being the electron mass and γ_1 is a Luttinger parameter [72,74]. (b) ZFSs as a function of electric field E_x for $L_z = 12$ nm. Inset: enlargement at small electric fields, where the main anisotropy axis changes from the wire axis (z) to the SOI axis (y).

where we also confirm the validity of our four subband model by comparing it to a full three-dimensional simulation.

In Fig. 2(a), we compare the numerical simulation of a Ge NW with $L = 10$ nm with the analytical formulas of the exchange splitting \mathcal{J} and the ZFS in Eq. (4) as a function of QD length L_z . In this calculation, the $\{x, y, z\}$ axes coincide with the $\langle 100 \rangle$ crystallographic directions. Strikingly, the numerical exchange splitting \mathcal{J} is in excellent agreement with the analytical formula, and also \mathcal{D} is reasonably well captured by the simple Eq. (4) in a wide range of QD sizes. We emphasize that due to the weak dependence of the coefficient η on the side length L in long QDs ($L, a_B < l_z$), Eq. (4) can accurately estimate the ZFS in general architectures.

The numerical solution in Fig. 2(a) also reveals an additional ZFS of the remaining two triplet states, that emerges because of the short-range corrections to the Coulomb interaction [36]. These corrections stem from the atomistic interactions of the p -type Bloch functions and induce mixing between the different bulk hole bands. The contribution of the short-range corrections to the effective Hamiltonian of Eq. (3) can be written as

$$H_{\text{eff,sr}} = \frac{1}{2} \mathcal{E} \sigma_1^z \sigma_2^z, \quad (6)$$

where \mathcal{E} is the exchange anisotropy along the NW (z direction). This ZFS induces an energy gap \mathcal{E} between the triplets $|T_0\rangle, |T_a\rangle = (|T_+\rangle + |T_-\rangle)/\sqrt{2}$ and the remaining states [the singlet $|S\rangle$ and the third triplet $|T_b\rangle = (|T_+\rangle - |T_-\rangle)/\sqrt{2}$], thereby lifting the remaining triplet degeneracy at zero magnetic field.

The exchange anisotropy \mathcal{E} induced by the short-range Coulomb interaction is also present without external electric fields, where the SOI vanishes [see Fig. 2(b)]. In

this special case, because of the fourfold symmetry of the system, the anisotropy axis is aligned to the wire [72,75,76]. If an electric field is applied perpendicular to the wire, the symmetry is reduced and the remaining degeneracy is also lifted. (For a detailed symmetry analysis of different wire geometries, see Sec. S3 of Ref. [72].) At small E_x , the ZFS \mathcal{D} increases quadratically with the electric field, because $v_3 \sim E_x$, and eventually overcomes \mathcal{E} [see the inset in Fig. 2(b)], aligning the main anisotropy axis to the SOI. For higher electric fields, v_3 (and thus \mathcal{D}) reaches a maximum value and starts to decrease, in analogy to the linear SOI v in various NW geometries [30,35].

The electric field dependence of the ZFS in Eq. (4) is dominated by v_3^2 and therefore \mathcal{D} is highly tunable by the external gate potentials and by the QD design. In particular, in Fig. 3 we show \mathcal{D} as a function of electric field in Ge and Si NWs for different growth directions. For both growth directions, the ZFS—relative to the orbital splitting—is significantly smaller in Si than in Ge. This reduction is a result of the hybridization of HHs and LHs with the spin-orbit split-off band that is much closer in Si ($\Delta_{\text{SO}} = 44$ meV) than in Ge ($\Delta_{\text{SO}} = 296$ meV) [74], effectively decreasing the HH-LH mixing and the SOI [35].

The ZFS also varies substantially between different growth directions for both materials, as shown in Fig. 3. The strong dependence of the SOI on the growth direction is well known in Si nanowires [30,35], and it is also significant in Ge. Strikingly, the linear SOI v changes only slightly in Ge between the two growth directions [30,39], but the cubic SOI v_3 is strongly altered between the two cases, yielding an order of magnitude larger ZFS when $x \parallel [110]$. This enhancement can be explained by considering that the cubic SOI is a higher-order correction that involves more subbands, making v_3 more sensitive to the growth direction and to the design of the QD. This finding stresses once again that the ZFS in hole QDs is induced by

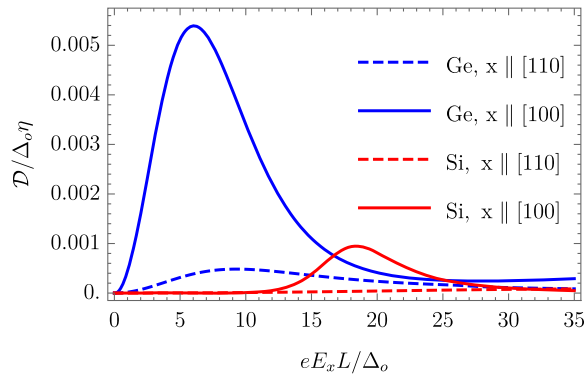


FIG. 3. Dependence of the ZFS \mathcal{D} in Eq. (4) on the electric field E_x . With blue (red) lines, we show Ge (Si) for two different growth directions and split-off gap $\Delta_{SO} \sim 150\Delta_o$ ($\Delta_{SO} \sim 4\Delta_o$). Here, we consider $l_z = L = 2a_B$, $z \parallel [001]$, and we use the strain $\epsilon_{zz} = -0.5\%$. The orbital energy is $\Delta_o = \hbar^2/m^*l_z^2$.

the cubic SOI v_3 and that there is no direct relation between the ZFS and the linear SOI v .

Conclusions.—We presented a simple analytical model explaining the large anomalous triplet splitting at zero magnetic field, emerging in QDs occupied by two holes and shedding some light on recent experimental findings [48]. We related the ZFS to a cubic SOI that is externally tunable by electric fields and can be engineered by the design of the QD. In striking contrast to linear SOI effects, the ZFS is found to depend significantly on the growth direction not only in Si but also in Ge QDs, where such anisotropic effects are typically small [8,30]. The SOI-induced ZFS is also found to be orders of magnitude larger than short-range corrections to the Coulomb interaction, an alternative mechanism for the ZFS of triplet states. While our analytical model focuses on doubly occupied long QDs, our findings are also valid in two tunnel-coupled QDs, the main building blocks of current spin-based quantum processors, and thus our work has deep implications for the design of future scalable quantum computing architectures with hole spin qubits.

We thank G. Katsaros, A. Pályi, and D. Miserev for fruitful discussions. This work was supported as a part of NCCR SPIN funded by the Swiss National Science Foundation (Grant No. 51NF40-180604).

*bence.hetenyi@unibas.ch

[1] D. Loss and D. P. DiVincenzo, *Phys. Rev. A* **57**, 120 (1998).
 [2] M. A. Eriksson, M. Friesen, S. N. Coppersmith, R. Joynt, L. J. Klein, K. Slinker, C. Tahan, P. M. Mooney, J. O. Chu, and S. J. Koester, *Quantum Inf. Process.* **3**, 133 (2004).
 [3] L. M. K. Vandersypen, H. Bluhm, J. S. Clarke, A. S. Dzurak, R. Ishihara, A. Morello, D. J. Reilly, L. R. Schreiber, and M. Veldhorst, *npj Quantum Inf.* **3**, 34 (2017).
 [4] G. Burkard, T. D. Ladd, J. M. Nichol, A. Pan, and J. R. Petta, [arXiv:2112.08863](https://arxiv.org/abs/2112.08863).

[5] L. Bellentani, M. Bina, S. Bonen, A. Secchi, A. Bertoni, S. P. Voinigescu, A. Padovani, L. Larcher, and F. Troiani, *Phys. Rev. Applied* **16**, 054034 (2021).
 [6] C. Kloeffel and D. Loss, *Annu. Rev. Condens. Matter Phys.* **4**, 51 (2013).
 [7] G. Scappucci, C. Kloeffel, F. A. Zwanenburg, D. Loss, M. Myronov, J.-J. Zhang, S. De Franceschi, G. Katsaros, and M. Veldhorst, *Nat. Rev. Mater.* **6**, 926 (2021).
 [8] C. Kloeffel, M. Trif, and D. Loss, *Phys. Rev. B* **84**, 195314 (2011).
 [9] L. A. Terrazos, E. Marcellina, Z. Wang, S. N. Coppersmith, M. Friesen, A. R. Hamilton, X. Hu, B. Koiller, A. L. Saraiva, D. Culcer, and R. B. Capaz, *Phys. Rev. B* **103**, 125201 (2021).
 [10] F. N. M. Froning, M. J. Rančić, B. Hetényi, S. Bosco, M. K. Rehmann, A. Li, E. P. A. M. Bakkers, F. A. Zwanenburg, D. Loss, D. M. Zumbühl, and F. R. Braakman, *Phys. Rev. Research* **3**, 013081 (2021).
 [11] H. Liu, T. Zhang, K. Wang, F. Gao, G. Xu, X. Zhang, S.-X. Li, G. Cao, T. Wang, J. Zhang, X. Hu, H.-O. Li, and G.-P. Guo, *Phys. Rev. Applied* **17**, 044052 (2022).
 [12] F. N. M. Froning, L. C. Camenzind, O. A. H. van der Molen, A. Li, E. P. A. M. Bakkers, D. M. Zumbühl, and F. R. Braakman, *Nat. Nanotechnol.* **16**, 308 (2021).
 [13] L. C. Camenzind, S. Geyer, A. Fuhrer, R. J. Warburton, D. M. Zumbühl, and A. V. Kuhlmann, *Nat. Electron.* **5**, 178 (2022).
 [14] S. D. Liles, F. Martins, D. S. Miserev, A. A. Kiselev, I. D. Thorvaldson, M. J. Rendell, I. K. Jin, F. E. Hudson, M. Veldhorst, K. M. Itoh, O. P. Sushkov, T. D. Ladd, A. S. Dzurak, and A. R. Hamilton, *Phys. Rev. B* **104**, 235303 (2021).
 [15] K. Wang, G. Xu, F. Gao, H. Liu, R.-L. Ma, X. Zhang, Z. Wang, G. Cao, T. Wang, J.-J. Zhang, D. Culcer, X. Hu, H.-W. Jiang, H.-O. Li, G.-C. Guo, and G.-P. Guo, *Nat. Commun.* **13**, 206 (2022).
 [16] C. Kloeffel, M. Trif, P. Stano, and D. Loss, *Phys. Rev. B* **88**, 241405(R) (2013).
 [17] P. M. Mutter and G. Burkard, *Phys. Rev. Research* **3**, 013194 (2021).
 [18] V. P. Michal, J. C. Abadillo-Uriel, S. Zihlmann, R. Maurand, Y.-M. Niquet, and M. Filippone, [arXiv:2204.00404](https://arxiv.org/abs/2204.00404).
 [19] S. Bosco, P. Scarlino, J. Klinovaja, and D. Loss, *Phys. Rev. Lett.* **129**, 066801 (2022).
 [20] S. Bosco and D. Loss, [arXiv:2204.08212](https://arxiv.org/abs/2204.08212).
 [21] N. W. Hendrickx, D. P. Franke, A. Sammak, M. Kouwenhoven, D. Sabbagh, L. Yeoh, R. Li, M. L. V. Tagliaferri, M. Virgilio, G. Capellini, G. Scappucci, and M. Veldhorst, *Nat. Commun.* **9**, 2835 (2018).
 [22] G. Scappucci, P. J. Taylor, J. R. Williams, T. Ginley, and S. Law, *MRS Bull.* **46**, 596 (2021).
 [23] L. Vukušić, J. Kukučka, H. Watzinger, J. M. Milem, F. Schäffler, and G. Katsaros, *Nano Lett.* **18**, 7141 (2018).
 [24] H. Watzinger, J. Kukučka, L. Vukušić, F. Gao, T. Wang, F. Schäffler, J.-J. Zhang, and G. Katsaros, *Nat. Commun.* **9**, 3902 (2018).
 [25] M. Urdampilleta, D. J. Niegemann, E. Chanrion, B. Jadot, C. Spence, P.-A. Mortemousque, C. Bäuerle, L. Hutin, B. Bertrand, S. Barraud, R. Maurand, M. Sanquer, X. Jehl,

- S. De Franceschi, M. Vinet, and T. Meunier, *Nat. Nanotechnol.* **14**, 737 (2019).
- [26] N. W. Hendrickx, W. I. L. Lawrie, L. Petit, A. Sammak, G. Scappucci, and M. Veldhorst, *Nat. Commun.* **11**, 3478 (2020).
- [27] A. Greilich, S. G. Carter, D. Kim, A. S. Bracker, and D. Gammon, *Nat. Photonics* **5**, 702 (2011).
- [28] N. W. Hendrickx, D. P. Franke, A. Sammak, G. Scappucci, and M. Veldhorst, *Nature (London)* **577**, 487 (2020).
- [29] N. W. Hendrickx, W. I. L. Lawrie, M. Russ, F. van Riggelen, S. L. de Snoo, R. N. Schouten, A. Sammak, G. Scappucci, and M. Veldhorst, *Nature (London)* **591**, 580 (2021).
- [30] C. Kloeffel, M. J. Rančić, and D. Loss, *Phys. Rev. B* **97**, 235422 (2018).
- [31] R. Winkler, D. Culcer, S. J. Papadakis, B. Habib, and M. Shayegan, *Semicond. Sci. Technol.* **23**, 114017 (2008).
- [32] R. Moriya, K. Sawano, Y. Hoshi, S. Masubuchi, Y. Shiraki, A. Wild, C. Neumann, G. Abstreiter, D. Bougeard, T. Koga, and T. Machida, *Phys. Rev. Lett.* **113**, 086601 (2014).
- [33] B. Hetényi, C. Kloeffel, and D. Loss, *Phys. Rev. Research* **2**, 033036 (2020).
- [34] J. Li, B. Venitucci, and Y.-M. Niquet, *Phys. Rev. B* **102**, 075415 (2020).
- [35] S. Bosco, B. Hetényi, and D. Loss, *PRX Quantum* **2**, 010348 (2021).
- [36] A. Secchi, L. Bellentani, A. Bertoni, and F. Troiani, *Phys. Rev. B* **104**, 205409 (2021).
- [37] S. Bosco and D. Loss, *Phys. Rev. Lett.* **127**, 190501 (2021).
- [38] D. V. Bulaev and D. Loss, *Phys. Rev. Lett.* **98**, 097202 (2007).
- [39] S. Bosco, M. Benito, C. Adelsberger, and D. Loss, *Phys. Rev. B* **104**, 115425 (2021).
- [40] Z. Wang, E. Marcellina, A. R. Hamilton, J. H. Cullen, S. Rogge, J. Salfi, and D. Culcer, *npj Quantum Inf.* **7**, 54 (2021).
- [41] N. Piot, B. Brun, V. Schmitt, S. Zihlmann, V. P. Michal, A. Apra, J. C. Abadillo-Uriel, X. Jehl, B. Bertrand, H. Niebojewski, L. Hutin, M. Vinet, M. Urdampilleta, T. Meunier, Y.-M. Niquet, R. Maurand, and S. De Franceschi, *arXiv:2201.08637*.
- [42] F. Maier, C. Kloeffel, and D. Loss, *Phys. Rev. B* **87**, 161305 (R) (2013).
- [43] A. Crippa, R. Maurand, L. Bourdet, D. Kotekar-Patil, A. Amisse, X. Jehl, M. Sanquer, R. Laviéville, H. Bohuslavskiy, L. Hutin, S. Barraud, M. Vinet, Y.-M. Niquet, and S. De Franceschi, *Phys. Rev. Lett.* **120**, 137702 (2018).
- [44] B. Venitucci, L. Bourdet, D. Pouzada, and Y.-M. Niquet, *Phys. Rev. B* **98**, 155319 (2018).
- [45] S. D. Liles, R. Li, C. H. Yang, F. E. Hudson, M. Veldhorst, A. S. Dzurak, and A. R. Hamilton, *Nat. Commun.* **9**, 3255 (2018).
- [46] S. Studenikin, M. Korkusinski, M. Takahashi, J. Ducatel, A. Padawer-Blatt, A. Bogan, D. G. Austing, L. Gaudreau, P. Zawadzki, A. Sachrajda, Y. Hirayama, L. Tracy, J. Reno, and T. Hargett, *Commun. Phys.* **2**, 159 (2019).
- [47] J. H. Qvist and J. Danon, *Phys. Rev. B* **105**, 075303 (2022).
- [48] G. Katsaros, J. Kukučka, L. Vukušić, H. Watzinger, F. Gao, T. Wang, J.-J. Zhang, and K. Held, *Nano Lett.* **20**, 5201 (2020).
- [49] J. Davidsson, V. Ivády, R. Armiento, N. T. Son, A. Gali, and I. A. Abrikosov, *New J. Phys.* **20**, 023035 (2018).
- [50] A. Lenef and S. C. Rand, *Phys. Rev. B* **53**, 13441 (1996).
- [51] J. R. Maze, A. Gali, E. Togan, Y. Chu, A. Trifonov, E. Kaxiras, and M. D. Lukin, *New J. Phys.* **13**, 025025 (2011).
- [52] P. Szakács, Á. Szabados, and P. R. Surján, *Chem. Phys. Lett.* **498**, 292 (2010).
- [53] D. Jirovec, A. Hofmann, A. Ballabio, P. M. Mutter, G. Tavani, M. Botifoll, A. Crippa, J. Kukučka, O. Sagi, F. Martins, J. Saez-Mollejo, I. Prieto, M. Borovkov, J. Arbiol, D. Christina, G. Isella, and G. Katsaros, *Nat. Mater.* **20**, 1106 (2021).
- [54] D. Jirovec, P. M. Mutter, A. Hofmann, A. Crippa, M. Rychetsky, D. L. Craig, J. Kukučka, F. Martins, A. Ballabio, N. Ares, D. Christina, G. Isella, G. Burkard, and G. Katsaros, *Phys. Rev. Lett.* **128**, 126803 (2022).
- [55] P. M. Mutter and G. Burkard, *Phys. Rev. B* **104**, 195421 (2021).
- [56] D. Fernandez-Fernandez, Y. Ban, and G. Platero, *arXiv:2204.07453*.
- [57] K. Ono, D. G. Austing, Y. Tokura, and S. Tarucha, *Science* **297**, 1313 (2002).
- [58] R. Li, F. E. Hudson, A. S. Dzurak, and A. R. Hamilton, *Nano Lett.* **15**, 7314 (2015).
- [59] G. Burkard, D. Loss, and D. P. DiVincenzo, *Phys. Rev. B* **59**, 2070 (1999).
- [60] H.-B. Braun and D. Loss, *Phys. Rev. B* **53**, 3237 (1996).
- [61] L. S. Levitov and E. I. Rashba, *Phys. Rev. B* **67**, 115324 (2003).
- [62] D. Stepanenko, M. Rudner, B. I. Halperin, and D. Loss, *Phys. Rev. B* **85**, 075416 (2012).
- [63] C. Satoko, in *Proceedings of the Institute of Natural Sciences* (Nihon University, Tokyo, 1990), p. 97.
- [64] M. Taut, *Phys. Rev. A* **48**, 3561 (1993).
- [65] J. C. Abadillo-Uriel, B. Martinez, M. Filippone, and Y.-M. Niquet, *Phys. Rev. B* **104**, 195305 (2021).
- [66] F. Gao, J.-H. Wang, H. Watzinger, H. Hu, M. J. Rančić, J.-Y. Zhang, T. Wang, Y. Yao, G.-L. Wang, J. Kukučka, L. Vukušić, C. Kloeffel, D. Loss, F. Liu, G. Katsaros, and J.-J. Zhang, *Adv. Mater.* **32**, 1906523 (2020).
- [67] H. E. Ercan, S. N. Coppersmith, and M. Friesen, *Phys. Rev. B* **104**, 235302 (2021).
- [68] A. Secchi, L. Bellentani, A. Bertoni, and F. Troiani, *Phys. Rev. B* **104**, 035302 (2021).
- [69] R. Maurand, X. Jehl, D. Kotekar-Patil, A. Corna, H. Bohuslavskiy, R. Laviéville, L. Hutin, S. Barraud, M. Vinet, M. Sanquer, and S. De Franceschi, *Nat. Commun.* **7**, 13575 (2016).
- [70] C. Adelsberger, M. Benito, S. Bosco, J. Klinovaja, and D. Loss, *Phys. Rev. B* **105**, 075308 (2022).
- [71] S. Bravyi, D. P. DiVincenzo, and D. Loss, *Ann. Phys. (Amsterdam)* **326**, 2793 (2011).
- [72] See Supplemental Material at <http://link.aps.org/supplemental/10.1103/PhysRevLett.129.116805> for an explicit derivation of the ZFS and further details of the numerical calculation. The symmetry analysis of the triplet degeneracy is also provided, as well as the exact form of the interband Coulomb corrections. Furthermore, we compare the numerical calculation for long QDs with a different numerical approach relying on a short QD assumption.

- [73] F. N. M. Froning, M. K. Rehmann, J. Ridderbos, M. Brauns, F. A. Zwanenburg, A. Li, E. P. A. M. Bakkers, D. M. Zumbühl, and F. R. Braakman, *Appl. Phys. Lett.* **113**, 073102 (2018).
- [74] R. Winkler, *Spin-Orbit Coupling Effects in Two-Dimensional Electron and Hole Systems* (Springer, New York, 2003), Vol. 191.
- [75] J. Sólyom, *Fundamentals of the Physics of Solids: Volume 1: Structure and Dynamics* (Springer Science & Business Media, Berlin, 2007), Vol. 1.
- [76] G. F. Koster, J. O. Dimmock, and R. G. Wheeler, *Properties of the Thirty-Two Point Groups* (MIT Press, Cambridge, MA, 1963), Vol. 24.